Guanine Binding Site of the *Nicotiana glutinosa* Ribonuclease NW Revealed by X-Ray Crystallography

Shin Kawano, Yoshimitsu Kakuta, and Makoto Kimura*

Laboratory of Biochemistry, Department of Bioscience and Biotechnology, Faculty of Agriculture, Graduate School, Kyushu University, Fukuoka 812-8581, Japan

Received June 7, 2002; Revised Manuscript Received September 5, 2002

ABSTRACT: Ribonuclease NW (RNase NW), the wound-inducible RNase in *Nicotiana glutinosa* leaves, preferentially cleaves guanylic acid. We expressed the cDNA encoding RNase NW in the methylotrophic yeast *Pichia pastoris* using the expression vector pPIC9K, and the resulting recombinant RNase NW (ryRNaseNW) secreted into medium was purified to apparent homogeneity using column chromatography. The crystal structure of ryRNase NW bound to 5′-GMP was determined at 1.5 Å resolution by molecular replacement with tomato RNase LE as a search model. The RNase NW structurally belongs to the ($\alpha + \beta$) class of proteins, having eight helices (five α-helices and three 3_{10} helices) and six β-strands, and its structure is highly similar to those of other plant RNases, including a uridylic acid preferential RNase MC1 from bitter gourd seeds. The guanine ring of 5′-GMP lies in a hydrophobic pocket of the molecular surface composed of Tyr17, Tyr71, Ala80, Leu79, and Phe89: the guanine base is sandwiched between aromatic side chains of Tyr17 and Phe89. In addition, the guanine base is firmly stabilized by a network of hydrogen bonds of the side chains of Gln12 and Thr78, as well as of the main chain of Leu79. Therefore, Gln12, Tyr17, Thr78, Leu79, and Phe89 are responsible for recognition of the guanine base by RNase NW, findings which provide insight into the manner in which RNase NW preferentially cleaves guanylic acid.

The 2′,3′-cyclizing ribonucleases (RNases) in mammalians as well as in microbial cells have been extensively studied and classified into three distinct families, RNase A, RNase T1, and RNase T2 families, according to molecular weights and amino acid sequences. As for base specificity, RNases belonging to the RNase T1 family specifically cleave guanylic acid (*1*), while RNases in the RNase A family cleave a phosphoester bond recognizing pyrimidine bases (*2*). Because of their restrictive substrate specificity, these RNases have become invaluable tools in molecular biological research. In contrast, RNases belonging to the RNase T2 family show unique base preferences with a nonabsolute base specificity (*3*). The biochemical characterization of this class of enzymes has not heretofore been pursued.

The RNase belonging to the RNase T2 family was initially purified from *Aspergillus oryzae* as an adenylic acid preferential RNase (*4*), and it is now known that RNases in the RNase T2 family are ubiquitous from viruses to human cells (*3*). The common properties of this class of enzymes are as follows: they are single polypeptide chains with about 200 amino acid residues and contain two common sequences CAS I and CAS II with two invariant histidine residues that are crucial for catalytic activity (*3*). The best characterized enzymes of the RNase T2 family is RNase Rh from *Rhizopus niveus*. RNase Rh comprises 222 amino acid residues with five disulfide bonds (*5*). The adenylic preferential (A > G > U, C) of RNase Rh was estimated based on the release of nucleotides from RNA during the course of hydrolysis (*6*). Kinetic and site-directed mutagenesis studies identified His46, His109, His104, Glu105, and Lys108 as catalytic amino acid residues; the former two histidine residues function as general acid and base catalysis in the transfer reaction (*7*, *8*, and references therein). The crystal structure of RNase Rh in a complex with 2′-AMP revealed that Trp49, Asp51, and Tyr57 are involved in interactions with the adenine base (*9*, *10*).

A large amount of sequence information is now available for plant RNases (*11*). Primary structures of plant RNases were found to be homologous to those of fungal RNases, including RNase T2 and RNase Rh; they are thus classified into the RNase T2 family (*11*). Enzymatic properties were examined on extracellular and vacuolar RNases from cultured tomato cells (*12*, *13*), as well as on seed RNases from Cucubitaceae, such as bitter gourd and sponge gourd (*14*). Analyses of seed RNases using dinucleoside monophosphates as substrates revealed an unique property of substrate

* Corresponding author. Address: Laboratory of Biochemistry, Department of Bioscience and Biotechnology, Faculty of Agriculture, Graduate School, Kyushu University, Hakozaki 6-10-1, Higashi-ku, Fukuoka 812-8581, Japan. Tel (fax): +81-92-642-2853. E-mail: mkimura@agr.kyushu-u.ac.jp.

[1] Abbreviations: 2′-AMP, 2′-monophosphate adenylic acid; 2′-UMP, 2′-monophosphate uridylic acid; 3′-UMP, 3′-monophosphate uridylic acid; 5′-GMP, 5′-monophosphate guanylic acid; dApC, deoxyadenyly-3′,5′ cytidine; HPLC, high performance liquid chromatography; NpU, nucleoside-3′,5′-uridine; rmsd, root-mean-square deviation; RNase, ribonuclease; RNase LE, RNase from cultured tomato (*Lycopersicon esculentum*); RNase MC1, RNase from bitter gourd (*Momordica charantia*); RNase NW, wound-inducible RNase from *N. glutinosa* leaves; reRNase NW, recombinant RNase NW in *Escherichia coli*; ryRNase NW, recombinant RNase NW in *Pichia pastoris*; RNase Rh, RNase from *Rhizopus niveus*; SDS−PAGE, sodium dodecyl sulfate−polyacrylamide gel electrophoresis; YNB, yeast nitrogen base.

10.1021/bi026247l CCC: $22.00
Published on Web 11/23/2002

specificity of plant RNases. Namely, the 2′,3′-cyclizing RNases have two distinct base binding sites, B1 site and B2 site, for bases located at the 5′- and 3′-terminal ends of a scissile bond. Base specificity usually relates to nature of the interaction of the B1 site with the base located at the 5′-terminal end. In contrast, the specificity of seed RNases was set by the uracil at the 3-terminal side of dinucleoside monophosphates, thereby suggesting the importance of the B2 site for substrate specificity for plant RNases (*14*). Furthermore, plant RNases are classified into two groups in terms of substrate preference: the tomato type is G > A > U > C, and the seed type is U > G > A > C (*14*). To better understand the structural basis for substrate preference of plant RNases, we determined earlier the crystal structure of the uridine-preferential bitter gourd RNase MC1 complexed with 2′-UMP and 3′-UMP (*15*). The structure, together with results obtained from site-directed mutagenesis (*16*), identified amino acid residues involved in recognition of the uracil base by RNase MC1.

We also purified a wound-inducible RNase NW from *Nicotiana glutinosa* leaves and characterized the enzymatic properties (*17*). RNase NW consists of 204 amino acids and shares 84% identical amino acids with RNase LE induced by phosphate starvation in tomato cultured cells (*13*). RNase NW preferentially cleaves polyinosinic acid among the homopolynucleotides, whereas polyadenylic acid was only slightly digested, and polyuridylic and polycytidylic acids were not affected. When the rates of hydrolysis were expressed as that of yeast RNA as 100, those of polyinosinic acid and polyadenylic acid were 96.5 and 8.8, respectively (*17*). These findings suggested that RNase NW belongs to guanylic acid preferential RNases. To gain more insight into the structural basis for the substrate preference of RNases in the RNases T2 family, we extended our structure analysis to the guanylic acid preferential RNase NW. For this purpose, we first constructed an overproduction system of RNase NW in the methanolytic yeast *Pichia pastoris*, and the recombinant RNase NW (ryRNase NW) in a complex with 5′-GMP was crystallized under 0.1 M Tris HCl, pH 8.5 containing 2.0 M ammonium dihydrogen phosphate. The X-ray crystallographic analysis of the crystal revealed that the guanine base interacts with Gln12 and Thr78 by hydrogen bondings and is further stabilized with Tyr17 and Phe89 by a sandwich-like stacking interaction. We now report the overproduction of RNase NW using the *P. pastoris* expression system and the three-dimensional structure of ryRNase NW complexed with 5′-GMP.

MATERIALS AND METHODS

Materials. The cDNA encoding RNase NW was previously cloned and sequenced (*17*). Multi-Copy Pichia Expression kits, including the expression plasmid pPIC9K and host strain GS115, were obtained from Invitrogen. DNA modification enzymes were obtained from MBI Fermentas. The oligonucleotide primers and plasmid pGEM T-vector were from Amersham Pharmacia Biotech. Guanine monophosphate was purchased from Sigma Chemical Co. All other reagents and chemicals were of analytical grade.

Expression and Purification of RNase NW. The cDNA fragment with artificial recognition sites of *Eco* RI and *Not* I at 5′- and 3′-ends, respectively, was amplified by PCR from the RNase NW cDNA, using sense TCAGTCCTTGAATTCGCTCAAGATTTCGAC and anti-sense GGCCGCGGCCGCTTAACTAAAATGTTGGGA primers (nucleotides underlined indicate recognition sites by *Eco* RI and *Not* I, respectively), and the resulting product was first ligated to the pGEM T-vector, by which *Esherichia coli* cell JM109 was transformed. The resulting T-vector harboring the PCR product was digested with *Eco* RI and *Not* I, and the resulting cDNA fragment was ligated to pPIC9K previously digested with the same restriction enzymes to obtain the expression plasmid pPIC9K−NW. Transformation of *P. pastoris* strain GS115 by pPIC9K−NW was carried out using a lithium chloride method, as suggested by the manufacturer of the *P. pastoris* expression system. Prior to transformation, pPIC9K−NW was linearized by restriction cleavage with *Bgl* II to stimulate homologous recombination at the *AOX*1 locus. RNase NW expression clones in GS115 were identified by their His^+ and Mut^s growth phenotype as described by the manufacturer. In addition, RNase NW expression clones were identified using indicator plates, as described (*18*). Six transformants expressing RNase NW were grown in 100 mL of BMGY medium (1% yeast extract, 2% peptone, 100 mM potassium phosphate, pH 6.0, 1.34% YNB, 4 × 10−5% biotin, 1% glycerol) for 2 days, and the culture was inoculated into 1 L of BMMY medium (1% yeast extract, 2% peptone, 100 mM potassium phosphate, pH 6.0, 1.34% YNB, 4 × 10−5% biotin, 0.5 ∼ 1% methano) at a density of OD600 = 1.0. The culture was grown at 30 °C for 5 days, and 100% methanol was added to a final concentration of 0.5−1.0% methanol every 24 h to maintain induction. After the growth medium had been centrifuged at 6000 rpm for 20 min, the supernatant was placed onto a Q-Sepharose Fast Flow column (1.5 × 20 mm) equilibrated with 10 mM Na-phosphate buffer, pH 8.0. The ryRNase NW was eluted with a linear gradient from 0 to 0.9 M NaCl concentration. The protein was further purified on a S−Sepharose column (1.5 × 20 mm) in 10 mM Na-acetate buffer, pH 5.0, and the protein was eluted with a linear gradient from 0 to 0.5 M NaCl. The purity of the protein was analyzed using SDS−PAGE (*19*) and N-terminal amino acid sequencing by gas-phase protein sequencer PSQ-1 (Shimadzu). Protein concentration was determined using a protein bicinconinic acid assay reagent (Pierce).

Crystallization. The ryRNase NW solution (10 mg/mL) in 10 mM Na−phosphate buffer, pH 7.0, was crystallized in the presence of 10 mM 5′-GMP using a hanging-drop vapor diffusion method. Crystal Screens I and II from Hampton Research were used to screen crystallization conditions for the ryRNase NW-5′-GMP complex. The hanging drops equilibrated over 1 mL of mother liquor at 18 °C. The crystals were obtained under conditions of numbers 46 and 48 of Crystal Screen I. At these conditions, crystals appeared within 2 days. The crystals used for data collection were from a drop of 2 μL of ryRNase NW and 10 mM 5′-GMP in 10 mM phosphate buffer, pH 7.0 with 2 μL of mother liquor (0.1 M Tris HCl, pH 8.5, containing 2.0 M ammonium dihydrogen phosphate).

Data Collection and Processing. The crystal was flash frozen by transferring to paratone-N liquid (Hampton Research). Diffraction data were collected using an oscillation method at 100 K on a Oxford CCD detector at beamline BL44XU of SPring-8, Japan. The crystal was orthrombic,

Table 1. Crystallographic Data and Refinement Statistics

Crystallographic Data	
space group	$P2_12_12_1$
unit cell parameters (Å)	$a = 44.8$, $b = 94.3$, $c = 98.1$
number of crystals	1
resolution (Å)	37.4−1.5
redundancy	5.6 (1.7)
R_{sym}[a]	0.052 (0.201)
$I/\zeta I$	11.6 (2.0)
completeness (%)	93.2 (53.8)
temperature (K)	100
beam line	SPring-8 BL44XU
Refinement Statistics	
R_{cryst}/R_{free} (%)[b]	21.2/23.0
number of reflections	62367
number of waters	435
rmsd from ideality	
bond lengths (Å)	0.005
bond angles (deg)	1.4
dihetral angles (deg)	23.4
improper angles (deg)	0.89

[a] $R_{sym} = \sum|I_i - \langle I\rangle|/\sum I_i$, where I_i is the intensity of the ith observation and $\langle I\rangle$ is the mean intensity of the reflection. [b] $R = \sum||F_o| - |F_c||/\sum|F_o|$, where R_{cryst} is calculated using the 95% of reflections used in refinement and R_{free} is calculated using the 5% held aside.

space group $P2_12_12_1$ with unit-cell dimensions of $a = 44.8$ Å, $b = 94.3$ Å, and $c = 98.1$ Å. Diffraction images were processed and scaled with d*TREK (*20*).

Structure Determination and Refinement. The structure of ryRNase NW in complex with 5′-GMP was determined using the molecular replacement method with CNS (*21*). The structure of RNase LE (PDB code, 1DIX), with 84% identity to the RNase NW in the amino acid sequence, served as a search model. The two ryRNase NW molecules could be located in the asymmetric unit, yielding a correlation coefficient of 0.616 and an *R* factor of 0.401. After protein atoms were refined by simulated annealing, we could clearly determine the position and conformation of the 5′-GMP in difference density maps. Refinement against 1.5 Å data was done using CNS with rounds of manual rebuilding in O (*22*). The stereochemical checks were carried out using PROCHECK (*23*). Diffraction and refinement statistics are given in Table 1. The atomic coordinates have been deposited in the Protein Data Bank under the accession code 1IYB.

Nomenclature for Substrate Binding Sites. RNases have the primary site and subsite for bases located at 5′- and 3′-terminal ends of the scissile bond. In this report, the primary and subsites are referred to as B1 and B2 sites, respectively, according to the nomenclature of RNase A (*24*).

RESULTS

Expression and Crystallization of RNase NW. The expression plasmid construct pPIC9K−NW was used to transform *P. pastoris* strain GS115. His^+ transformants were selected and screened for expression of RNase NW by indicator plates, as described under Materials and methods. Clones positive for RNase NW expression were identified at a frequency between 10% and 20% of His^+ transformants, and levels of protein expression were in general similar in independent clones. In all cases, SDS−PAGE analysis showed that the positive GS115 strains secreted the protein into the medium, which produced a band of approximately 22-kDa protein (data not shown). The ryRNase NW thus

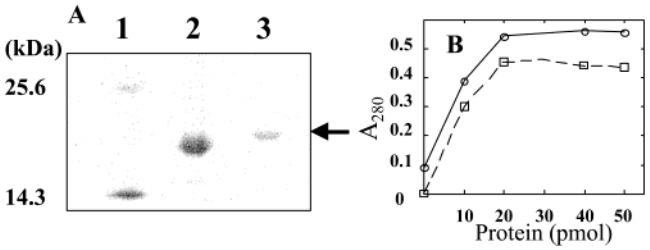

FIGURE 1: Expression of RNase NW in the yeast *Pichia pastoris.* The cDNA fragment encoding mature RNase NW was expressed by the *P. pastoris* expression system, as described under Materials and Method. (A) SDS−PAGE of the purified ryRNase NW. Lane 1, maker proteins α-chymotrypsinogen (25.6 kDa) and lysozyme (14.3 kDa); lane 2, reRNase NW; lane 3, ryRNase NW. The arrow indicates the position of ryRNase NW. (B) RNA degradation activity of ryRNase NW (○) and reRNase NW (□). Enzymatic activity of enzymes was assessed by following the increase in acid-soluble nucleotides after digestion of yeast RNA at pH 6.5 and 37 °C, as described by Ohgi et al. (*37*). The absorbency of the supernatant after centrifugation was measured at 260 nm.

produced was purified, as described under Materials and methods. The purified ryRNase NW gave a single band on SDS−PAGE (Figure 1A), which moved slightly slower than that of the recombinant RNase NW (reRNase NW) produced in *E. coli* cells. The direct N-terminal sequencing provided a single sequence: Tyr-Val-Glu-Phe-Ala-Gln. This result indicated a specific cleavage by the STE13 gene product at the peptide bond between Ala and Tyr in the α-factor signal sequence, giving rise to ryRNase NW which has an extra four amino acid sequence (Tyr-Val-Glu-Phe) attached to the N-terminal amino acid residue of RNase NW. The potential for ryRNase NW to cleave RNA was examined using yeast RNA as a substrate. The ryRNase NW cleaved yeast RNA slightly stronger than did reRNase NW produced in *E. coli* cells (Figure 1B).

Crystal Structure Analysis. The crystal structure of ryRNase NW complexed with 5′-GMP was determined at 1.5 Å resolution by molecular replacement with the tomato RNase LE (*25*) as a search model. There are two crystallographically independent molecules, making up the asymmetric unit of the ryRNase NW crystals, which are denoted as molecules A and B. The intermolecular contact involves residues Ser52−Asn53 in the two molecules, forming antiparallel strands by hydrogen bonding interactions (Figure 2). Since ryRNase NW appeared to be monomeric in solution, as judged by findings on the gel filtration column (data not shown), it is likely that the occurrence of molecules A and B in the asymmetric unit is due to a crystallographic artifact. The final electron density map is of high quality and thus facilitated atomic modeling of all 208 amino acid residues and 5′-GMP bound to molecules A and B (Figure 3). The structure was refined at 1.5 Å resolution to a final *R*-factor of 21.2% ($R_{free} = 23.0\%$). The rmsd from standard values (*26*) of bond lengths and angles are 0.005 Å and 1.4°, respectively. There are no major differences between molecules A and B except for the extra signal sequences; 202 Cα atoms of the two molecules (Asp3−Phe204) are superimposed with an rmsd of 0.471 Å determined using the program O. Although there is a good electron density for extra signal peptides (Tyr-Val-Glu-Phe) in the two molecules, the relative orientation of the extra peptide to the mature molecules differs between molecules A and B. Signal peptides in both molecules protrude from the surface of the

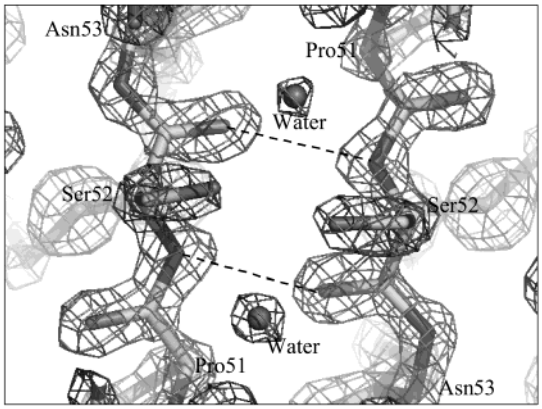

FIGURE 2: Part of the 1.5 Å resolution electron density map. The figure indicates part of the electron density maps of molecules A and B in asymmetric unit of the ryRNase NW crystals. The figure was drawn using PyMol (http://www.pymol.org).

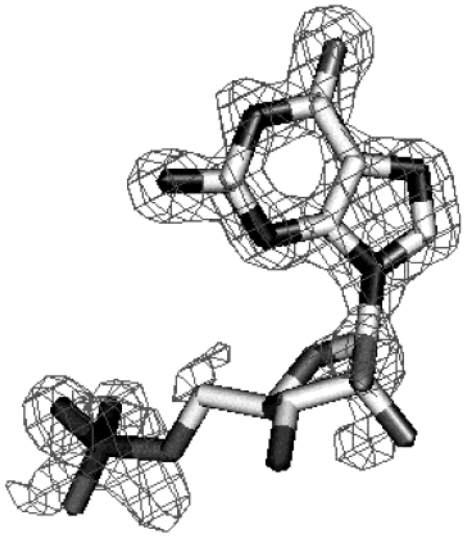

FIGURE 3: The electron density map of 5′-GMP bound to RNase NW. The difference Fourier map is calculated with coefficients of $(F_{complex} - F_{native}) \exp(i\alpha c)$. Contours are drawn at the 3.5σ level. $F_{complex}$ and F_{native} are observed structure factors of RNase NW−5′-GMP complex and RNase LE crystals, respectively. αc is the phase angle calculated from RNase LE.

molecules, forming strong hydrogen bonds with amino acid main chains from positions Ser23 to Tyr26 on an adjacent symmetry-related molecule. It is thus likely that the different conformation observed for the two peptides relates to crystal packing of the molecules.

Overall Structure of RNase NW. The three-dimensional structure of ryRNase NW in a complex with 5′-GMP is shown in Figure 4. Secondary elements of ryRNase NW, as defined by the DSS Program (*27*), are given in Figure 5. ryRNase NW is composed of eight α helices (α1−α8) and six β strands (β1−β6) characteristic of the α + β type structure. The amino acid residues (β1, 6−12; and β2, 37−43) at the N-terminal region form a two-stranded antiparallel β-sheet, intervening one 3_{10} helix (α1, 14−16) and loop structures. The polypeptide enters the extended helical structures (α2, 61−66; α3, 68−74; α4,87−95; α5, 97−100; α6, 106−119; and α7, 122−128), having a short β strand (β3, 137−139) followed by α-helix (α8, 140−152). The amino acid residues at the C-terminal region form an antiparallel β-sheet (β4, 157−162; and β5, 168−178), forming a central antiparallel pleated β-sheet with the

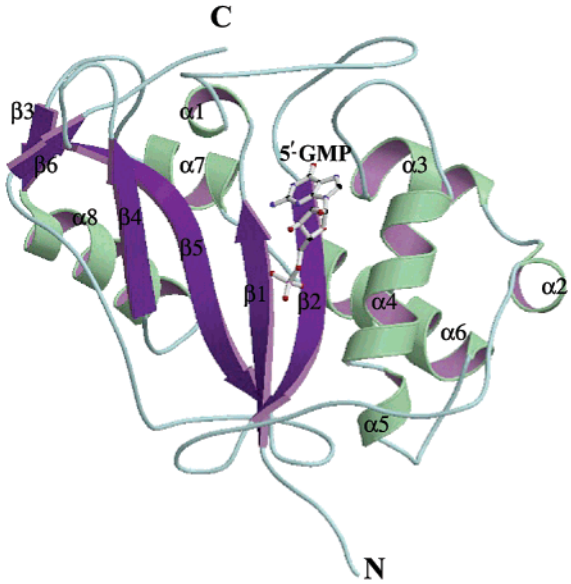

FIGURE 4: Ribbon representation of RNase NW in complex with 5′-GMP. The view is not drawn on the noncrystallographic 2-fold axis. α-helices and β-strands are indicated in light green and violet, respectively, and loops are shown in white. The structure was drawn using Molscript (*38*).

N-terminal β-strands (β1−β3). The structure is completed by β-strand (β6, 198−200) preceding by a long loop structure. The overall structure of ryRNase NW has a significant similarity to those of other known plant RNases, RNase LE and RNase MC1. A structural superposition of the Cα atoms in the entire ryRNase NW with RNase LE, determined using the program O, gave rmsd value of 0.68 Å, and the rmsd, calculated only for structurally related 160 Cα atoms of ryRNase NW and RNase MC1 was 2.02 Å.

5′-GMP Bound to RNase NW. A comparison of 5′-GMP structures in molecules A and B shows virtually a similar conformation. The side chains of residues that make a specific interaction with the guanine base are Gln12, Tyr17, Thr78, and Phe89 (Figure 6). The side chains $N^{\delta 2}$ and $O^{\delta 1}$ of Gln12 interact with O6 (2.51 Å) and N1 (2.79 Å) atoms of the guanine base as hydrogen acceptor and donor, respectively, and the hydroxyl group of Thr78 donates a hydrogen bond to the N7 (3.03 Å) atom of the guanine base. In addition, the main chain NH group of Leu79 is hydrogen-bonded to the O6 (2.80 Å) atom of the guanine base. The guanine moiety is stabilized further in the hydrophobic pocket via a sandwich-like stacking interaction with two aromatic side chains of Tyr17 and Phe89. The aromatic ring of Phe89 is oriented in parallel to the guanine base at 3.50 Å distance, and that of Tyr17 covers the base at angle of 26 ° from 4.75 Å distance. Hydrogen bonding and stacking interactions with the guanine base provide insight into how RNase NW preferentially cleaves guanylic acid.

DISCUSSION

The wound-inducible RNase NW from the *N. glutinosa* is classified into guanylic acid preferential RNases, including RNase LE from tomato cultured cells, in terms of base-preference. To better understand the molecular basis for the guanylic acid preference for RNase NW, we analyzed the crystal structure of ryRNase NW in the presence of 5′-GMP. For this purpose, we attempted to construct an efficient

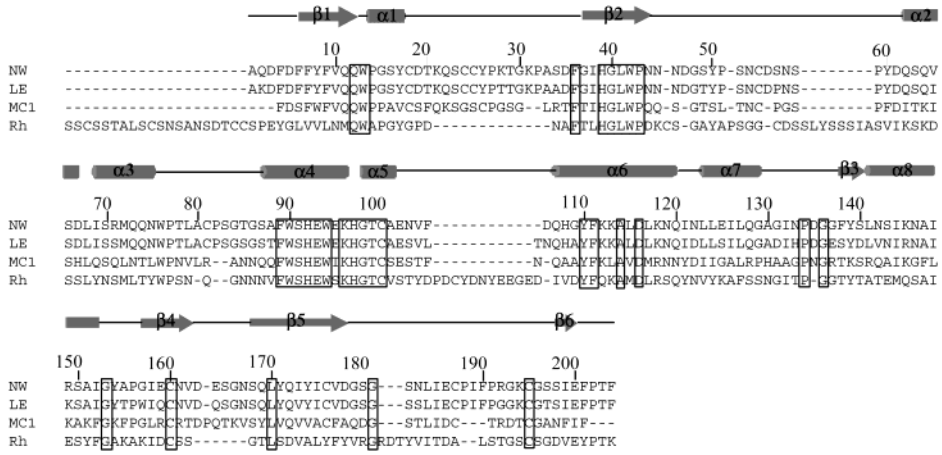

FIGURE 5: Sequence alignment of RNase NW and other T2 family RNases. The secondary structure elements indicated are those defined using the program DSSP. α-helices and 3_{10}-helices are indicated by bars. *β*-strands are indicated by arrows. The amino acid residues identical in RNases are enclosed in boxes. NW, LE, MC1, and Rh indicate amino acid sequences of RNase NW (*17*), RNase LE (*13*), RNase MC1 (*39*), and RNase Rh (*5*), respectively.

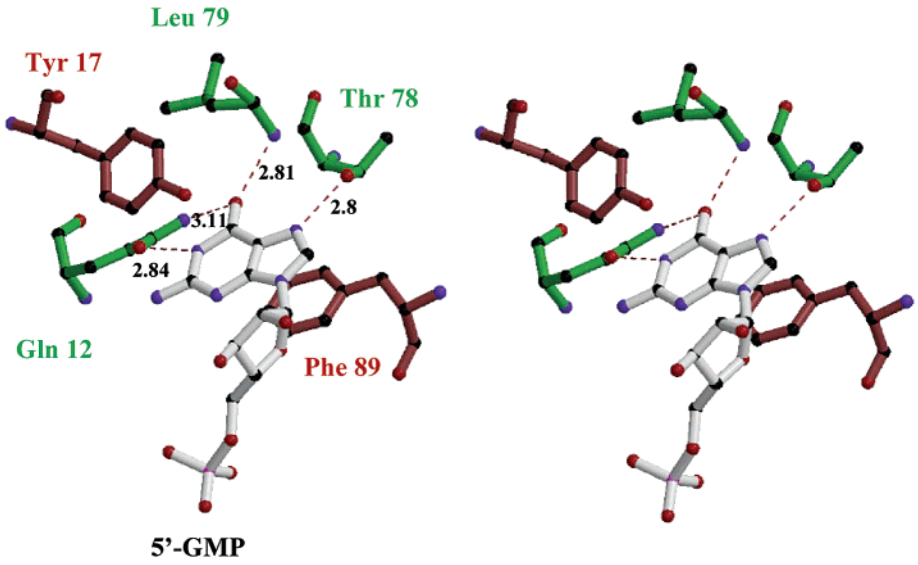

FIGURE 6: Stereoview of hydrogen bonding network of the RNase NW and 5′-GMP complex. The 5′-GMP is drawn in gray, and carbon, nitrogen, and oxygen atoms are in black, blue, and red, respectively. Amino acids Tyr17 and Phe89 involved in stacking interaction are in brown, and amino acids Gln12, Thr78, and Leu79 involved in hydrogen bonding are in green.

expression system for RNase NW. RNases are in general potentially toxic products for living cells if produced intracellularly in an active form. Therefore, attempts to secrete RNases with a signal sequence into the growth medium were undertaken. Indeed, bacterial RNases as well as mammalian RNases were expressed at very high levels when using *E. coli* secretion systems (*28*−*30*). Taking these findings into consideration, we previously constructed the *E. coli* expression system for RNase NW using pET-22b as an expression plasmid (*31*). In this system, the recombinant RNase NW (reRNase NW) could be secreted into the *E. coli* periplasmic space with the aid of the *pel B* signal sequence and characterized in terms of enzymatic properties. However, the yields were extremely low: less than 1 mg protein per liter of cultured cells (*31*). Similar low level accumulations in the *E. coli* expression system were noted for RNase MC1 and its mutant enzymes (*32*, *33*). Since inactive RNase MC1 mutants were produced in the same amount as wild-type RNase MC1, the low level accumulation of RNases in *E. coli* cells cannot be attributed to RNA degrading activity. It is likely that the low level expression of RNase NW and RNase MC1 in the *E. coli* systems is due to a distinct codon usage of plant RNase genes from bacteria genes.

Recently, we became aware that RNase A could be secreted into the growth medium using the methylotrophic yeast *P. pastoris*, and the enzymes thus obtained exhibited the same activity as the authentic enzyme (*34*). Hence, we attempted in the present study to express the cDNA encoding RNase NW in *P. pastoris*, using the expression plasmid pPIC9K. In the construct, the cDNA encoding the mature RNase NW is located as a downstream fusion to α-factor signal sequence gene preceded by the alcohol oxidase gene *AOX1* promoter, the objective being to secrete recombinant protein into the medium. As anticipated, ryRNase NW was abundantly expressed and secreted into the medium: the yield was about 50 mg per 1 L of cultured cells. The ryRNase NW thus obtained showed a slight stronger enzymatic activity than did reRNase NW produced in *E. coli* cells. A plausible explanation for the slight different enzymatic activity between ryRNase NW and reRNase NW is that it may be due to distinct methods of purifications. Namely, the ryRNase NW was purified by mild conditions using ion-

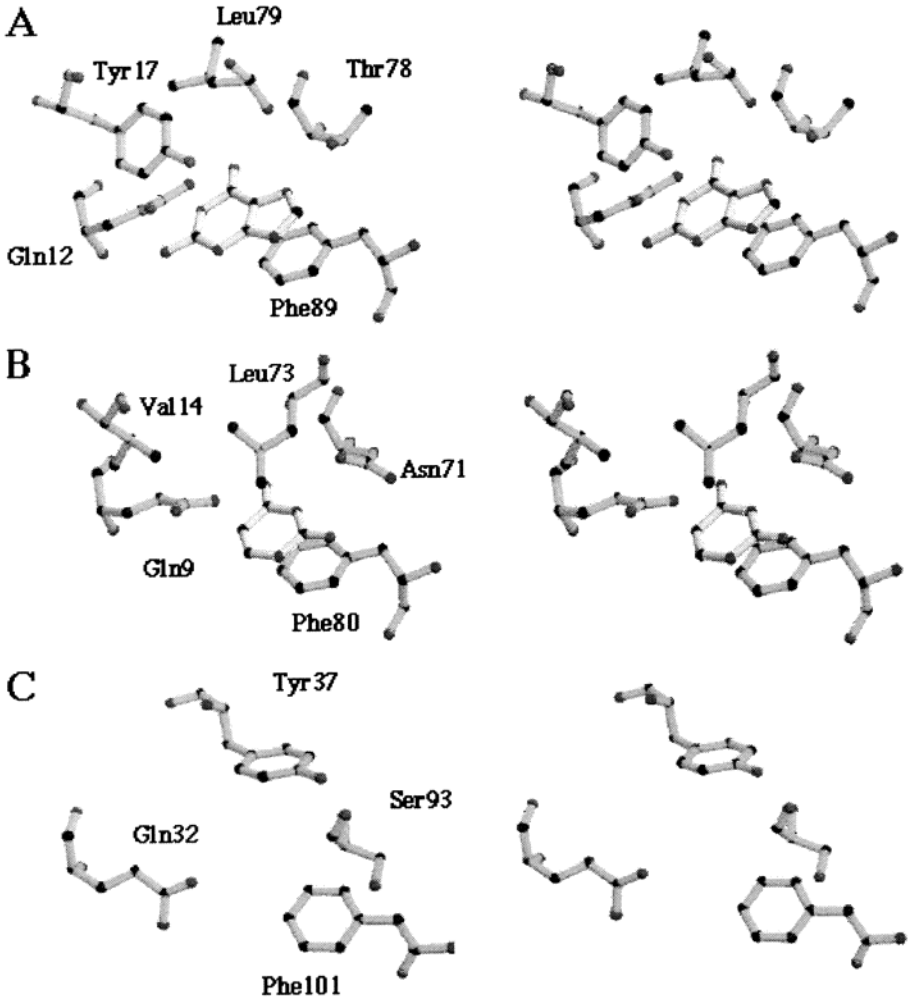

FIGURE 7: Conformations of amino acid residues composed of B2 site in the RNase T2 family. A, B, and C show stereoviews of conformations of amino acid residues composed of B 2 sites of RNase NW, RNase MC1, and RNase Rh, respectively. Guanine and uracil bases are shown in the B2 sites in RNase NW and RNase MC1. Structures of RNase MC1 and RNase Rh were cited from refs *15* and *9*, respectively.

exchange column chromatography as presented in this paper, while reRNase NW was finally purified by reverse-phase HPLC using acetonitrile in 0.1% trifluoroacetic acid as the solution (*31*). Probably, the reRNase NW was partly inactivated during purification on reverse-phase HPLC.

In the crystal structure of ryRNase NW-5′-GMP complex, the guanine moiety is fixed to the B2 site via stacking interactions between the aromatic side chains of Tyr17 and Phe89. It was reported that stacking interactions between exposed aromatic side chains and nonbase-paired RNA nucleotides is a common feature in a protein-RNA complex (*35*). Furthermore, the aromatic stacking with guanine base was also noted on a guanosine-specific microbial RNase T1. The crystallographic data on RNase T1 show that specific recognition of guanosine by RNase T1 involves sandwich-like parallel stacking of the guanosine base between the phenolic side chains of Tyr42 and Tyr45. Face-to-face stacking between Tyr42 and the guanine base was reported to significantly contribute to incremental binding energy of the substrate (*36*). It seems likely that the sandwich-like parallel stacking of the guanine base by the aromatic rings of Tyr17 and Phe89 plays an essential role in guanine binding to the B2 site in RNase NW. In addition to stacking interaction, the guanine base is hydrogen bonded to the side chains of Gln12 and Thr78. The C6 carbonyl and N1 hydrogen of guanine interacts favorably with the side chain of Gln12 as hydrogen acceptor and donor, respectively. As described in ref *17*, RNase NW preferentially cleaves polyinosinic acid, while polyadenosine is only slightly digested. The hydrogen bonding interactions provided by Gln12 is obviously unavailable for interaction with the adenine base. It is thus assumed that the discrimination against the adenine base is achieved through interactions of the side chain of Gln12 with C6 and N1 atoms in the guanine base.

RNases belonging to the RNase T2 family are distinct from RNases classified into RNase A and RNase T1 families in that they have a nonabsolute base specificity (*3*). It is known that RNases in the RNase T2 family have unique base preferences in the release of mononucleotides from RNA, the rates of hydrolysis of four homopolynucleotides, and the rates of hydrolysis of diribonucleoside monophosphates. On the basis of these findings, RNases in the RNase T2 family are classified into three groups, adenylic acid preferential (fungal type), such as RNase Rh, uridylic acid preferential (seed type), such as RNase MC1, and guanylic acid preferential (tomato type), such as RNase NW (*14*). Nakamura and co-workers determined crystal structures of adenylic acid preferential RNase Rh in the complex with 2′-AMP or dApC and assigned Trp49, Asp51, and Tyr57 and Gln31, Pro92, Ser93, Asn94, Gln95, and Phe101 as building blocks to constitute B1 site and B2 site, respectively (*3*, *9*, *10*). We

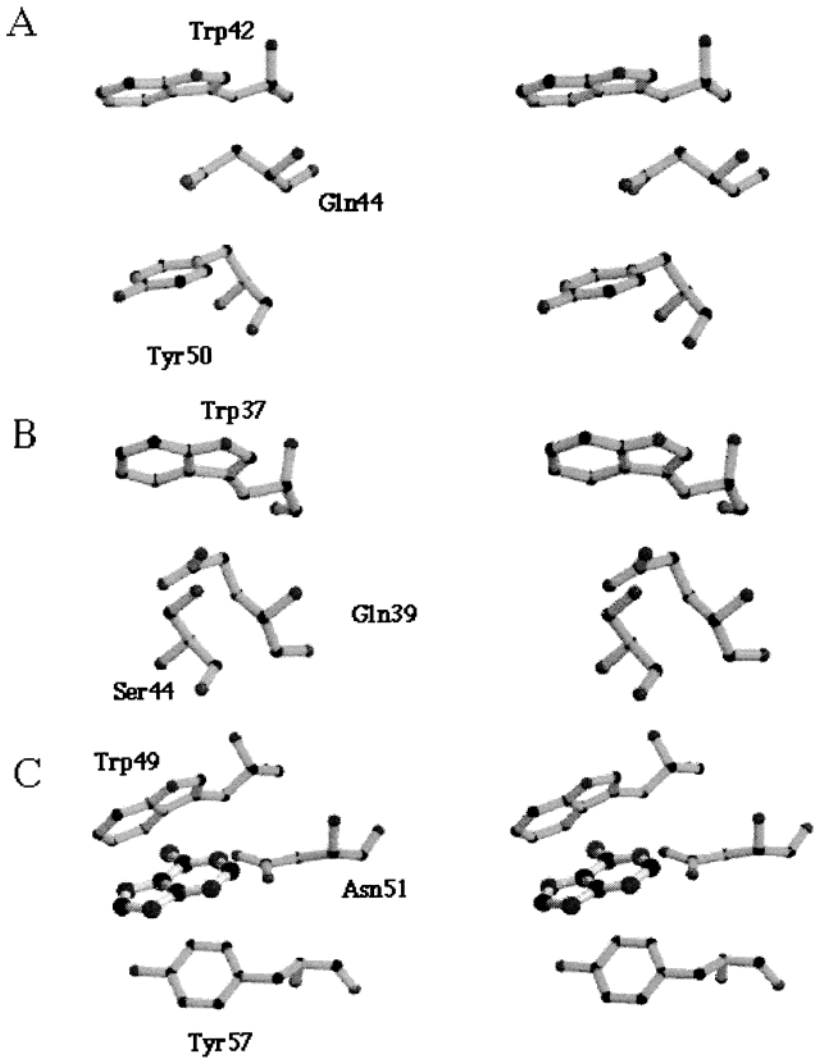

FIGURE 8: Conformations of amino acid residues composed of B1 site in the RNase T2 family. A, B, and C show stereoviews of conformations of amino acid residues composed of B 1 sites of RNase NW, RNase MC1, and RNase Rh, respectively. Adenine base is shown at the B1 site of RNase Rh (*9*).

recently determined the crystal structures of the uridylic acid preferential RNase MC1 complexed with 2′- or 3′-UMP (*15*) and found that side chains of Gln9 and Asn71 and the main chain of Val72 interact with the uracil base by hydrogen bondings. In addition, the uracil was sandwiched by the hydrophobic side chains of Leu73 and Phe80. Elucidation of the crystal structure of the guanylic acid preferential RNase NW in complex with 5′-GMP presented in this paper facilitated a comparison among substrate binding sites in all three RNase T2 family groups, as described below.

As described in Introduction, the uridylic acid preferential RNase MC1 isolated from bitter gourd seeds preferentially cleaves the P−O5′ ester bond of NpU (where N is either A, C, G, or U). In the RNase MC1−UMP complex structures, the uracil moiety was specifically fixed to the B2 site via a sandwich-like stacking interaction between the hydrophobic side chains of Leu73 and Phe80 and by an extensive network of hydrogen bonds (Figure 7B). Examining the structure of the ryRNase NW−5-GMP complex, the guanine base specifically lies on the B2 site, where Gln12, Thr78, and Leu79 are involved in hydrogen bondings to the guanine base, and Tyr17 and Phe89 sandwiched the guanine base by a face-to face stacking interaction (Figure 7A). Amino acid residues Gln12, Thr78, Leu79, and Phe89 in RNase NW correspond to Gln9, Asn71, Val72, and Phe80 in RNase MC1, respectively, and equivalently function in the RNase NW and 5′-GMP interactions. However, the sandwich-like stacking interaction by aromatic side chains Tyr17 and Phe89 in RNase NW is substituted with that by Leu73 and Phe80 in RNase MC1. Moreover, the substitution of a longer side chain of Asn71 in RNase MC1 with a shorter side chain of Thr78 in RNase NW enlarges the B2 space in RNase NW. It is thus suggested that an enlargement of the B2 space and the face to face stacking interactions provided by Tyr17 and Phe89 in RNase NW may render a guanine preference to RNase NW. As for the adenylic acid preferential RNase Rh, the amino acid residues Pro92, Ser93, Asn94, Gln95, and Phe101 are involved in the substrate binding at the B2 site, as described above (Figure 7C). In this interaction, Tyr17 and Leu73 which occurred in RNase NW and RNase MC1, respectively, are missing in RNase Rh. It is likely that the lack of a sandwich-like interaction at the B2 site in RNase Rh may decrease binding affinity of the substrate to the B2 site.

As for the B1 site in RNase Rh, the crystallographic study identified Trp49, Asp51, and Tyr57 as amino acids at the B1 site (Figure 8C). Comparing these amino acid residues with the corresponding residues in RNase NW, they are

highly conserved as Trp42, Asn44, and Tyr50 in RNase NW (Figure 8A). It is thus likely that Trp42, Asn44, and Tyr50 in RNase NW may be involved in substrate binding at the B1 site in RNase NW. In this context, it seems reasonable that RNase NW is active toward diribonucleoside monophosphate ApG (*30*). On the other hand, Asp51 and Tyr57 in RNase Rh are replaced by Gln39 and Ser44, respectively, in RNase MC1, although Trp42 in RNase Rh is conserved in RNase MC1 (Trp37) (Figure 8B). In particular, replacement of Tyr57 in RNase Rh with Ser44 in RNase MC1 results in the lack of a hydrophobic pocket, which is involved in adenine recognition at the B1 site in RNase Rh. RNase MC1 preferentially cleaves the phosphodiester bond of NpU (N denotes either A, C, or U) (*14*). It is speculated that the lack of rigid base recognition at the 5′-terminal end may render uracil preferential for RNase MC1.

CONCLUSION

The crystallographic study on ryRNase NW in complex with 5′-GMP indicated that amino acid residues Gln12, Tyr17, Thr78, Leu79, and Phe89 are involved in guanine binding. When these amino acids are compared with corresponding residues in RNases in the RNase T2 family, Gln12, Tyr17, and Phe89 are conserved in RNases in the family, while Thr78 and Leu79 at the loop between α3 and α4 helices in RNase NW are only conserved in the guanosine preferential RNases. It is thus assumed that interactions of the side chain of Thr78 and the backbone of Leu79 with the guanine base are responsible for the guanylic acid preferential of RNase NW. Indeed, the mutation of Asn71 in RNase MC1 by the corresponding amino acid Thr78 in RNase NW altered the substrate specificity from uridine preferential to guanosine preferential as shown by the transphosphorylation of dinucleoside monophosphates (*16*). Thus, it is concluded that the amino acid residues, in particular Thr78 (RNase NW numbering), at the loop between α3 and α4 play an essential role in substrate specificity for RNases in the RNase T2 family.

ACKNOWLEDGMENT

We are grateful to M. Ohara (Fukuoka) for helpful comments on the manuscript.

REFERENCES

1. Steyaert, J. (1997) *Eur. J. Biochem. 247*, 1−11.
2. delCardayre, S. B., and Raines, R. T. (1994) *Biochemistry 33*, 6031−6037.
3. Irie, M. (1999) *Pharmacol. Ther. 81*, 77−89.
4. Sato, K., and Egami, F. (1957*) J. Biochem. 44*, 753−767.
5. Horiuchi, H., Yanai, K., Takagi, M., Yano, K., Wakabayashi, E., Sanda, A., Mine, S., Ohgi, K., and Irie, M. (1988) *J. Biochem. 103*, 408−418.
6. Tomoyeda, M., Eto, Y., and Yoshino, T. (1969) *Arch. Biochem. Biophys. 131*, 191−202.
7. Ohgi, K., Horiuchi, H., Iwama, M., Watanabe, H., Takagi, M., and Irie, M. (1992) *J. Biochem. 112*, 132−138.
8. Irie, M., Ohgi, K., Iwama, M., Koizumi, M., Sasayama, E., Harada, K., Yano, Y., Udogawa, J., and Kawasaki, M. (1997) *J. Biochem. 121*, 849−853.
9. Kurihara, H., Nonaka, T., Mitsui, Y., Ohgi, K., Irie, M., and Nakamura, K. (1996) *J. Mol. Biol. 255*, 310−320.
10. Nakamura, K., Ishikawa, N., Hamashima, M., Kurihara, H., Nonaka, T., Mitsui, Y., Ohgi, K., and Irie, M. (1993) in *The 3rd International Meeting on Ribonuclease, Chemistry, Biology, Biotechnology*, Capri, p 5.
11. Green, P. J. (1994) *Annu. Rev. Plant Physiol. Plant Mol. Biol. 45*, 421−445.
12. Abel, S., Krauss, G.-J., and Glund, K. (1989) *Biochim. Biophys. Acta 998*, 145−150.
13. Nurnberger, T., Abel, S., Jost, W., and Glund, K. (1990) *Plant Physiol. 92*, 970−976.
14. Irie, M., Watanabe, H., Ohgi, K., Minami, Y., Yamada, H., and Funatsu, G. (1993) *Biosci. Biotechnol. Biochem. 57*, 497−498.
15. Suzuki, A., Yao, M., Tanaka, I., Numata, T., Kikukawa, S., Yamasaki, N., and Kimura, M. (2000) *Biochem. Biophys. Res. Commun. 275*, 572−576.
16. Numata, T., Suzuki, A., Yao, M., Tanaka, I., and Kimura, M. (2001) *Biochemistry 40*, 524−530.
17. Kariu, T., Sano, K., Shimokawa, H., Itoh, R., Yamasaki, N., and Kimura, M. (1998) *Biosci. Biotechnol. Biochem. 62*, 1144−1151.
18. Quaas, R., Landt, O., Grunert, H.-P., Beineke, M., and Hahn, U. (1989) *Nucleic Acids Res. 17*, 3318.
19. Laemmli, U.K. (1970) *Nature 227*, 680−685.
20. Pflugrath, J. W. (1999) *Acta Crystallogr., Sect. D 55*, 1718−1725.
21. Brunger, A. T., Adams, P. D., Clore, G. M., Delano, W. L., Gros, P., Grosse-Kunstleve, R. W., Jiang, J.-S., Kuszewski, J., Nilges, M., Pann, N. S., Read, R. J., Rice, L. M., Simonson, T., and Warren, G. L. (1998) *Acta Crystallogr., Sect. D 54*, 905−921.
22. Jones, T. A., Zou, J., Cowan, S., and Kjeldgaard, M. (1991) *Acta Crystallogr., Sect. A 47*, 110−119.
23. Lascowski, R. A., McArthur, M. W., Moss, D. S., and Thornton, J. M. (1993) *J. Appl. Crystallogr. 26*, 282−291.
24. Richards, F. M., and Wyckoff, H. W. (1971) *Enzymes (3rd Ed.) 4*, 647−806.
25. Tanaka, N., Arai, J., Inokuchi, N., Koyama, T., Ohgi, K., Irie, M., and Nakamura, K. (2000) *J. Mol. Biol. 298*, 859−873.
26. Engh, R. A., and Huber, R. (1991) *Acta Crystallogr., Sect. A 47*, 392−400.
27. Kabsch, W., and Sander, C. (1983) *Biopolymers 22*, 2577−2637.
28. Hartley, R. W. (1988) *J. Mol. Biol. 202*, 913−915.
29. Nambiar, K. P., Stackhouse, J., Presnell, S. R., and Benner, S. A. (1987) *Eur. J. Biochem. 163*, 67−71.
30. Ikehara, M., Ohtsuka, E., Tokunaga, T., Nishikawa, S., Uesugi, S., Tanaka, T., Aoyama, Y., Kikyodani, S., Fujimoto, K., Yanase, K., Fuchimura, K., and Morioka, H. (1986) *Proc. Natl. Acad. Sci. U.S.A. 83*, 4695−4699.
31. Hino, M., Kawano, S., and Kimura, M. (2002) *Biosci. Biotechnol. Biochem. 66*, 910−912.
32. Numata, T., Kashiba, T., Hino, M., Funatsu, G., Ishiguro, M., Yamasaki, N., and Kimura, M. (2000) *Biosci. Biotechnol. Biochem. 64*, 603−605.
33. Numata, T., and Kimura, M. (2001) *J. Biochem. 130*, 621−626.
34. Chatani, E., Tanimizu, N., Ueno, H., and Hayashi, R. (2000) *Biosci. Biotechnol. Biochem. 64*, 2437−2444.
35. Burd, C. G., and Dreyfuss, G. (1994) *Science 265*, 615−621.
36. Loverix, S., Doumen, J., and Steyaert, J. (1997) *J. Biol. Chem. 272*, 9653−9639.
37. Ohgi, K., Horiuchi, H., Watanabe H., Takagi, M., Yano, K., and Irie, M. (1991) *J. Biochem. 109*, 776−785.
38. Kraulis, P. J. (1991) *J. Appl. Crystallogr. 24*, 946−950.
39. Ide, H., Kimura, M., Arai, M., and Funatsu, G. (1991) *FEBS Lett. 284*, 161−164.

BI026247L